Accepted Manuscript of Mandal et. al. *Joule,* 3(1-12) DOI: 10.1016/j.joule.2019.09.016.

Porous Polymers with Switchable Optical Transmittance for Optical and Thermal Regulation

(Version accepted for publication in *Joule*, 3(1-12) https://doi.org/10.1016/j.joule.2019.09.016)

Jyotirmoy Mandal,[1] Mingxin Jia,[2] Adam Overvig,[1] Yanke Fu,[1] Eric Che,[3] Nanfang Yu,[1] and Yuan Yang[1]*

[1] Department of Applied Physics and Applied Mathematics, Columbia University, New York, NY, USA

[2] Department of Mechanical Engineering, Columbia University, New York, NY, USA

[3] Hunter College, City University of New York, New York, NY, USA

Summary: Adaptive control of broadband light is essential for diverse applications including building energy management and light modulation. Here, we present porous polymer coatings (PPCs) whose optical transmittance changes upon reversible wetting with common liquids, as a platform for optical management from solar to thermal wavelengths. In the solar wavelengths, reduction in optical scattering upon wetting changes PPCs from reflective to transparent. For poly(vinylidene fluoride-co-hexafluoropropene) PPCs, this corresponds to solar and visible transmittance changes of up to 0.74 and 0.80. For infrared (IR) transparent polyethylene PPCs, wetting causes an 'icehouse-to-greenhouse' transition where solar transparency rises but thermal IR transparency falls. These performances are either unprecedented, or rival or surpass those of notable optical switching (e.g. electrochromic, thermochromic) paradigms, making PPCs promising for large-scale optical and thermal management. Specifically, switchable sub-ambient radiative cooling (by 3.2˚C) and above-ambient solar heating (by 21.4˚C), color-neutral daylighting, and thermal camouflage are demonstrated.

Introduction

Porous polymer coatings (PPCs), which vary in their intrinsic optical properties and morphology, have recently gained prominence as a platform for optical and thermal management. For instance, solar-reflective and thermally emissive PPCs have been demonstrated as efficient radiative coolers.[1,2] Solar-reflective but thermally transparent PPCs, meanwhile, have been used as covers in devices with tuneable infrared (IR) emittances or for radiative cooling.[3–5] However, such PPCs are themselves optically static, which limits their use in radiatively dynamic environments (e.g. radiative coolers are desirable during summers, but not winters). If PPCs are made optically dynamic, they can be used for a much wider range of applications, such as tunable solar heating or radiative cooling of buildings and modulating light transmission through windows. However, PPCs with switchable optical properties in the solar and thermal wavelengths remain to be explored in detail.

In this work, we demonstrate that such optical dynamicity can be achieved by reversibly wetting PPCs with fluids like alcohol or water. For instance, white poly(vinylidene fluoride-co-hexafluoropropene) (P(VdF-HFP)) PPCs turn transparent upon wetting with refractive index-matched fluids like isopropanol (Fig. 1A-B, Video S1), showing large hemispherical (diffuse) transmittance (T) changes in the solar ($\Delta T_{sol}\sim 0.74$) and visible ($\Delta T_{vis}\sim 0.80$) wavelengths (Fig. 1C). Similar phenomena are observed for polytetrafluoroethene (PTFE), ethyl-cellulose and polyethylene (PE) (Fig 1F) PPCs. Furthermore, thermally transparent PE PPCs show a decrease in infrared (IR), specifically long-wavelength infrared (LWIR, $\lambda\sim 8-13\,\mu m$) transmittance (T_{LWIR}) when wetted with IR-emissive/absorptive alcohols (Fig. 1D-E). The contrasting $\Delta T_{LWIR}\sim -0.64$ and $\Delta T_{sol}\sim +0.33$ for PE PPCs represent a potentially unprecedented icehouse (low T_{sol}, high T_{LWIR}) to greenhouse (high T_{sol}, low T_{LWIR}) transition (Fig. 1F). We further show that PPC-based devices can achieve complete optical switching in ~ 1 minute and essentially unchanged performance after 100 wet-dry cycles. Promisingly, these performances are obtained with relative simplicity and inexpensiveness, making PPCs with fluid-mediated optical switching a scalable and energy-efficient paradigm for diverse applications such as controlling daylight in buildings, tunable solar heating and radiative cooling, and thermal camouflage.

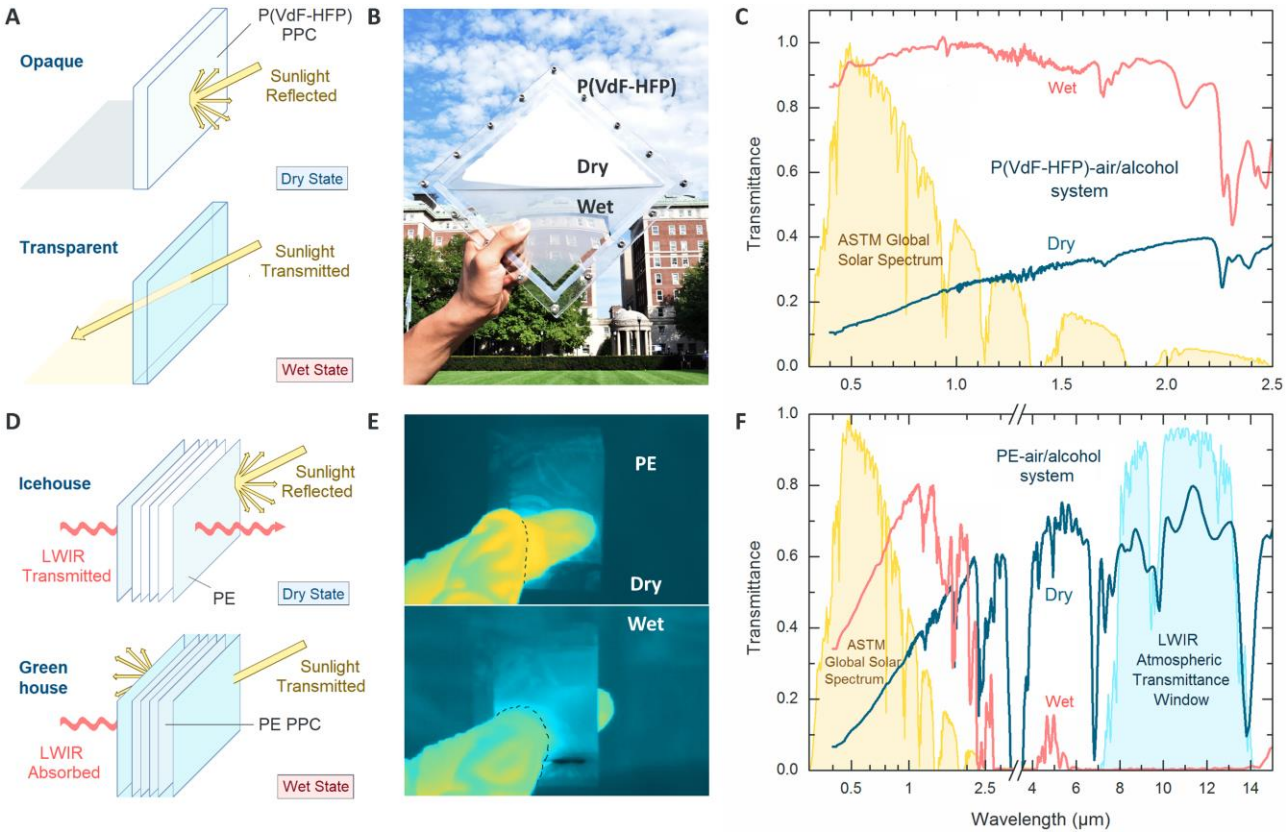

Figure 1. Optical switching of PPCs as exemplified by P(VdF-HFP) and PE. (A). White to transparent switching of the porous P(VdF-HFP)-air/isopropanol system. (**B)** Photograph of the system showing dry and wet states. **(C)** Spectral hemispherical transmittance of the wet and dry states, corresponding to a ΔT_{sol}~0.74 and ΔT_{vis}~ 0.80. **(D)** Icehouse to greenhouse switching of PPCs, exemplified by a PE-air/alcohol system. **(E)** LWIR thermographs of PE PPCs enclosed in PE films when dry and wetted with alcohol. Details are provided in Figure S1. **(F)** Spectral hemispherical transmittance of the wet and dry states of the PE-air/alcohol system, corresponding to a ΔT_{sol}~ 0.33 and $\Delta T_{LWIR} \sim -0.64$.

Results

Mechanisms of Optical Switching, exemplified by P(VdF-HFP) and PE

The contrasting optical switching behaviors of PPCs in the solar (Fig 1A-C) and thermal IR (Fig 1D-F) wavelengths arises from their different intrinsic optical properties and switching mechanisms in each wavelength range. The first type of transition, from reflective to transparent in the solar wavelengths (λ~0.4-2.5 μm) (Fig. 1C,F), arises from two factors – the intrinsic non-absorptivity of the polymers,[1,6] and a change in the refractive index (n) contrast ($\Delta n = n_{polymer} - n_{pores}$) across the polymer-pore boundaries (Fig. 2A-B) when the air in the pores is replaced by a liquid. This is exemplified by the P(VdF-HFP)-air/isopropanol system (Fig. 1B). P(VdF-HFP) (–[CF_2-CF_2]$_n$–[CF(CF_3)-CF_2]$_m$–), a saturated polymer, contains strong C-C and C-F bonds whose excitation energies are higher than photon energies in the solar wavelengths. Consequently, P(VdF-HFP) does not absorb sunlight. When structured into a hierarchically porous form, the polymer contains nano- and micropores with sizes between ~0.1 and ~10 μm within it (Fig. 2A).[1] In its dry state, the porous P(VdF-HFP) has a large solar $\Delta n\ (= n_{P(VdF-HFP)} - n_{air} = 1.40 - 1 = 0.40)$ across the polymer-pore boundaries, causing the pores to efficiently scatter solar wavelengths, and in the absence of any intrinsic absorption, yield a bright white appearance (Fig. 1B). Spectral reflectance shows that shorter, visible wavelengths are particularly well-reflected (Fig. 1C). This is corroborated by finite-difference-time-domain (FDTD) simulations, which show that large pores with sizes ~ 10 μm scatter all solar wavelengths, while smaller pores ~ 0.1 μm scatter shorter wavelengths better (Fig. 2C). However, when the pores are wetted with isopropanol (n ~ 1.38), a drastic reduction in $\Delta n\ (= n_{P(VdF-HFP)} - n_{isopropanol} = 1.40 - 1.38 = 0.02)$ causes the scattering efficiency of the pores to drop by one or more orders of magnitude (Fig. 2C). Consequently, solar transmittance T_{sol} and visible transmittance T_{vis} rises from 0.20 to 0.94

(ΔT_{sol}~0.74) and 0.13 to 0.93 (ΔT_{vis}~0.80), respectively (Fig. 1C). Angular measurements appear to show that while the dry state has a highly diffuse, almost Lambertian transmittance, the wet state's transmittance is primarily ballistic (Fig. 2D, upper panel), which manifests in the transparent appearance of thin (< 100 μm), wet porous P(VdF-HFP) films (Fig. 1B). Thicker, wet films are more translucent, indicating that diffuse transmittance is significant.

Translucency also increases with Δn in the wet state. This is observed in PE-air/isopropanol systems. PE (–[CH_2-CH_2]$_n$–), which is another solar non-absorptive polymer owing to its strong C-C and C-H bonds, has a solar refractive index of ~ 1.51. Consequently, it has an appreciable solar Δn ($= n_{PE} - n_{isopropanol} = 1.51 - 1.38 = 0.13$) when wet, which yields a diffuse transmittance and translucent appearance (Fig. 2D, lower panel and S2). For such a system, ΔT_{sol} observed with 160 μm thick PE PPCs, is 0.33 (Fig. S3). However, when oil (n~1.47) is used instead of isopropanol, a lower Δn leads to a higher transparency and ΔT_{sol} of 0.51 (Fig. S2). With even better refractive index matching, a ballistic transmittance for the wet state, and high ΔT_{sol} and ΔT_{vis}, as observed for P(VdF-HFP)-air/isopropanol systems, can be achieved.

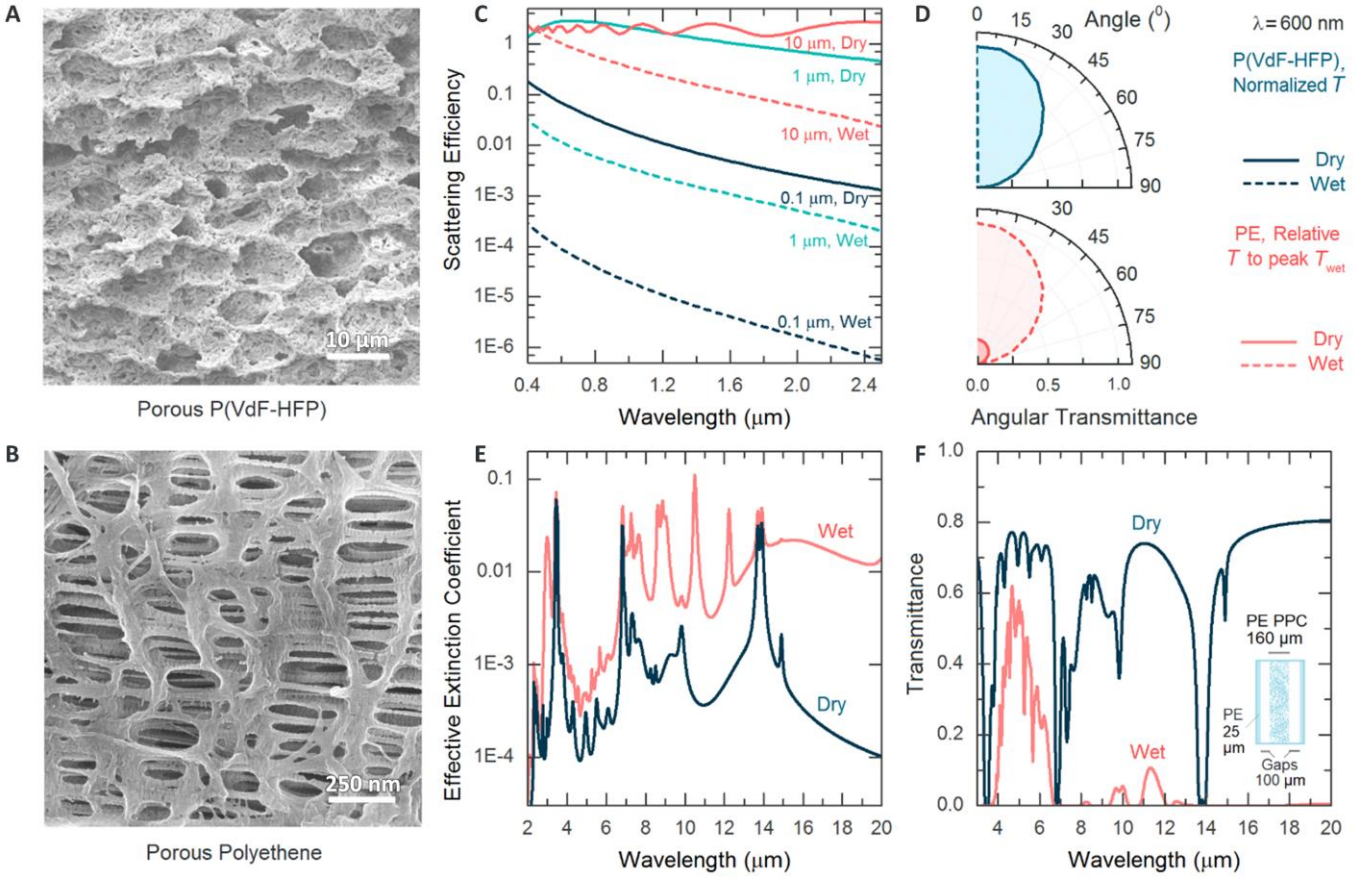

Figure 2. The optical switching mechanisms of PPCs. **(A)** Scanning electron micrograph of porous P(VdF-HFP), showing its nano- and microscale pores, and **(B)** of nanoporous polyethylene. **(C)** Scattering efficiencies of pores of different sizes in porous P(VdF-HFP) when dry and wet. Upon wetting, the scattering efficiencies drop by 10^1-10^3, causing a white to transparent transition. **(D)** Measured angular transmittance of wet and dry P(VdF-HFP) PPCs normalized to their respective peak angular values, and of wet and dry PE PPCs normalized to the peak wet angular transmittance. The transmittance for the wet P(VdF-HFP) PPC (Δn~0.02) appears to be ballistic, while that for wet PE-PPC (Δn~0.13) is diffuse. The angular transmittances of the dry states are diffuse and almost Lambertian, as expected from the large Δn (~$0.4 - 0.5$). **(E)** Effective electromagnetic extinction coefficients of PE PPCs when dry and wet with alcohol. As shown, the LWIR extinction coefficients rise by 10^1-10^2 upon wetting, causing the PE PPCs to change from LWIR transparent to absorptive/emissive. **(F)** Simulated transmittance of a PE-air/alcohol system containing a 160 μm thick PE PPC (inset). The transmission across the MWIR, LWIR and FIR wavelengths changes drastically when the enclosure is filled with alcohol.

The second type of transition, from transparent to opaque, is observed in the thermal IR wavelengths (λ~2.5-20 μm) when IR-transparent PPCs are wetted with intrinsically IR-absorptive/emissive liquids. The porous PE-air/alcohol system is an ideal example. Unlike typical polymers, which have multiple excitation modes across the IR wavelengths,[1,6,7] PE has only a few such modes (corresponding to its C-C and C-H bonds at ~ 3.4, 6.8 and 14.9 μm), none of which are in the LWIR atmospheric transmittance window. Consequently, nanoporous PE PPCs (Fig. 2B), which have ~ 40% porosity and pore sizes (~0.1 μm) too small to scatter thermal IR wavelengths, act as a highly IR-transparent effective medium with a low electromagnetic extinction coefficient κ (Figs. 1F, 2E). However, when wetted with IR-absorptive/emissive fluids such as alcohols, the PPCs become IR-absorptive/emissive as well (Fig. 1F). Specifically, their effective κ rises by ~10^1-10^2 in the LWIR wavelengths (Fig. 2E). Consequently, PE-air/alcohol systems (Fig. 2F, inset) can almost completely absorb LWIR radiation when wet, and show large $\Delta T_{LWIR} = T_{Dry} - T_{Wet} \sim 0.64 - 0.003 = 0.64$ (Figs. 1F and S3). According to Kirchhoff's law, the change in LWIR absorptance (ΔT_{LWIR}) corresponds to an equal change in LWIR emittance ($\Delta\epsilon_{LWIR}$). Similar transitions from transmissive to absorptive/emissive states also occur in the mid-wavelength infrared (MWIR, $\lambda \sim 3 - 5\ \mu m$) and far infrared (FIR, $\lambda \sim 15 - 20\ \mu m$) bands, while T_{sol} rises by 0.33 for 160 μm thick PPCs (Figs. 1F and 2F). These results are notable because firstly, the large, broadband thermal ΔT for $\lambda \sim 4 - 20\ \mu m$, and in particular the ΔT_{LWIR}~0.64, rank among the highest reported performances.[3,8–12] Secondly, the contrasting ΔT_{solar}~0.33 and $\Delta T_{\mathrm{LWIR}} \sim -\Delta\epsilon_{LWIR} \sim -0.64$ represents an icehouse to greenhouse transition that is, to our knowledge, the first reported instance in the literature, and different from the monotonic switching usually observed across the solar and thermal wavelengths with other designs.[3,11,13,14]

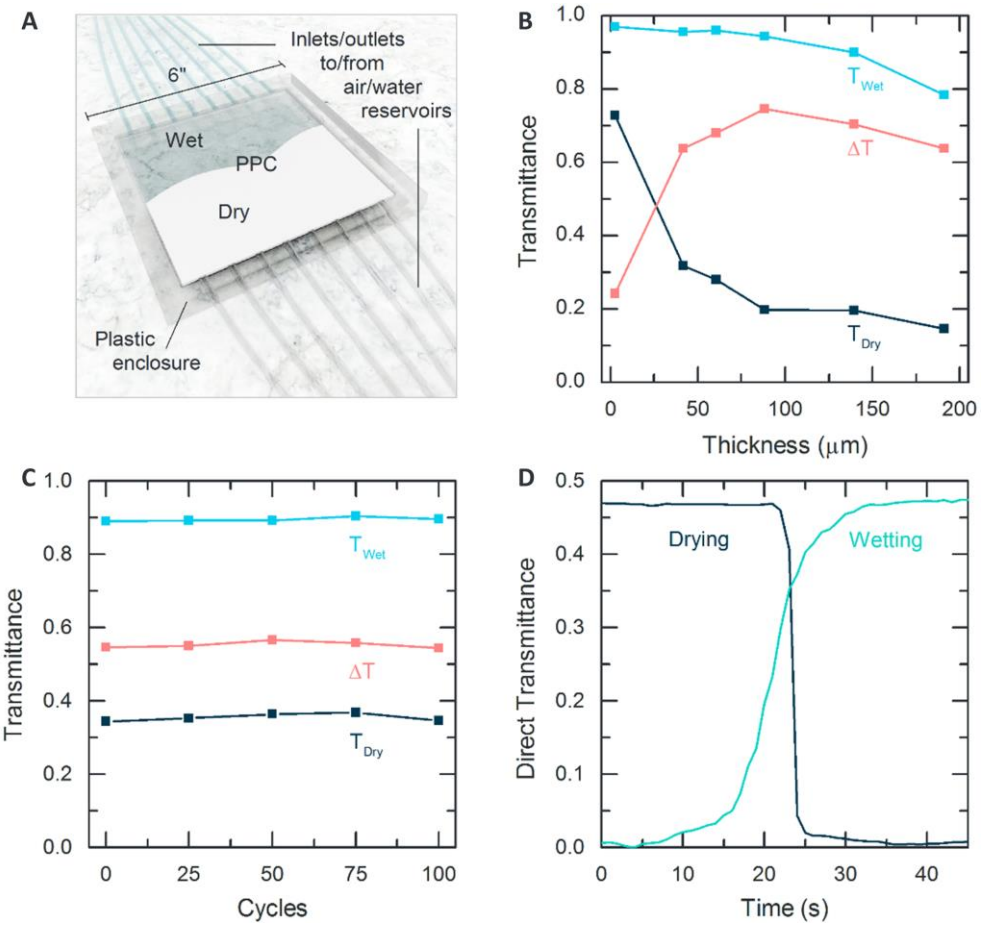

Figure 3. A P(VdF-HFP)-air/isopropanol system (A) Schematic shown during a dry to wet transition. **(B)** Effect of PPC thickness and **(C)** long-term cycling on solar transmittance of the devices. **(D)** Variation in direct transmittance, corresponding to ΔT_{sol}~0.74, of a device during wetting/drying with time, showing complete cycling in < 1 minute.

Device Performance of PPC-air/liquid Systems

The switchable optical transmittance of PPCs can be readily harnessed by appropriate device designs. In this paper, P(VdF-HFP) PPCs coated on inner surfaces of double-glazed plastic enclosures is used as a model system that is generalizable to other PPCs. As schematically shown in Fig. 3A, a 150 mm x 150 mm porous P(VdF-HFP) coating is pre-painted onto an inner surface of the enclosure (with a 2 mm gap) by a simple phase-inversion technique,[1] and is wetted by injecting isopropanol or dried by blowing air through the tubes. Such a device can be conveniently mounted on surfaces of objects (e.g. windows, roofs, and walls of buildings) requiring optical or thermal modulation.

To optimize and characterize the performance of the device in Fig. 3A, the effect of PPC thickness on ΔT, and the switching speed and long-term stability were investigated. As shown in Fig. 3B, with increasing thickness of P(VdF-HFP) PPCs, T_{sol} of the dry state drops rapidly due to increased optical scattering, reaching ~0.2 at thicknesses ~100 μm, and then drops more gradually. For the wet state, where scattering is greatly reduced, T_{sol} starts to significantly drop only at thicknesses beyond 100 μm. Consequently, a peak ΔT_{sol}~0.74 and ΔT_{vis}~0.80 are observed for a thickness of ~ 100 μm. Similar trends are observed for PE PPCs as well (Fig. S3).

The porous P(VdF-HFP)-based device also shows remarkably consistent performance over many wet-dry cycles. Even after 100 cycles, $T_{sol,dry}$, $T_{sol,wet}$ and ΔT_{sol} only show small changes of 0.343 → 0.346, 0.889 → 0.895 and 0.546 → 0.543 (Fig. 3C). The small differences observed could be due to spatial variations within the coating and experimental uncertainties associated with the optical measurements. The results indicate that repeated wetting and drying has no significant impact on the performance of the coatings. Furthermore, P(VdF-HFP) and PE PPCs are also found to be stable under wetting, solar illumination and heating over 8-day or longer periods (Table S1). Together, these results underscore the suitability of the coatings for prolonged use.

The porous P(VdF-HFP)-based device also shows fast switching speeds. As shown in Fig. 3D, a 110 μm thick P(VdF-HFP) PPC can become fully wet and transparent in ~ 30 s and fully dry and white in as little as ~ 15 s. The total cycling time, conservatively estimated at < 1 minute, is comparable with electrochromic systems, and indicates the suitability of our design for smart windows (Videos S2 and 3).[8,13,15] For large devices, optimizing the design to ensure fast switching remains to be explored in detail. Potential solutions include using modular designs and larger enclosure gaps that enable faster airflow (Supplemental Information, Section 5). However, for very large structures like rooftops or building facades which might need switching over diurnal or seasonal timescales, switching times ~ 1 hour or ~ 1 day respectively can be conveniently achieved with our design. Additionally, fast, energy efficient switching can be achieved with mechanically or gravitationally driven flows, and the fluids involved can be collected and recycled with further engineering.

Although alcohols such as isopropanol yield an excellent ΔT_{sol} owing to their near-ideal index match with P(VdF-HFP) PPCs, their flammability and environmental impact may pose a risk. Where this is prohibitive, using non-flammable isopropanol-water mixtures (Video S4) can significantly reduce or eliminate fire hazards and reduce potential environmental impact in case of device failure, while providing a ΔT_{sol} that is ~80% of their isopropanol-based counterpart's (Supplemental Information, Section 6). Another solution is hydrophilic PPCs such as ethyl cellulose, which switch upon wetting with water (Figs. 4 and S4, Table S2). Lastly, when alcohols are used, engineering controls such as the use of nitrogen for drying, addition of flame retardants to alcohol and the device walls, design of narrow enclosures that reduce the amount of combustible alcohol or air, and designs to prevent leakage, could be implemented to maximize safety.

Discussion

Diversity of PPCs and their Applications

While the demonstrations with P(VdF-HFP) and PE show the optical functionality and device compatibility of PPCs, they are but two examples from a wide variety of commonly available and inexpensive polymers from which PPCs can be made. Porous polymers are either commercially available, or easily fabricable at low costs and large scales using processes like phase inversion.[1,16] Besides P(VdF-HFP), PPCs exhibiting large ΔT_{sol} could be made using poly(vinylidene fluoride), poly(methyl-methacrylate), ethyl-cellulose and polystyrene,[1,17] and can exhibit switchable T_{sol} with appropriate fluids.[17] For thermal switching, poly(propylene) and nylon, which are appreciably transparent in the LWIR, may be used besides poly(ethylene).[4] Table S2 shows a variety of PPCs, ranging from commercially available poly(tetrafluoroethene) (PTFE) to paper sheets, which are suitable for large scale use. Furthermore, the enclosures for PPC-based devices (Fig. 3A) can be easily constructed using plastics or glass to yield good optical performance (Fig. 1B and Video S3). Collectively, these attributes make PPCs promising for a range of applications. In this section, we use four types of PPCs – P(VdF-HFP), PTFE, ethyl-cellulose and PE, and demonstrate the diversity of polymers and their uses.

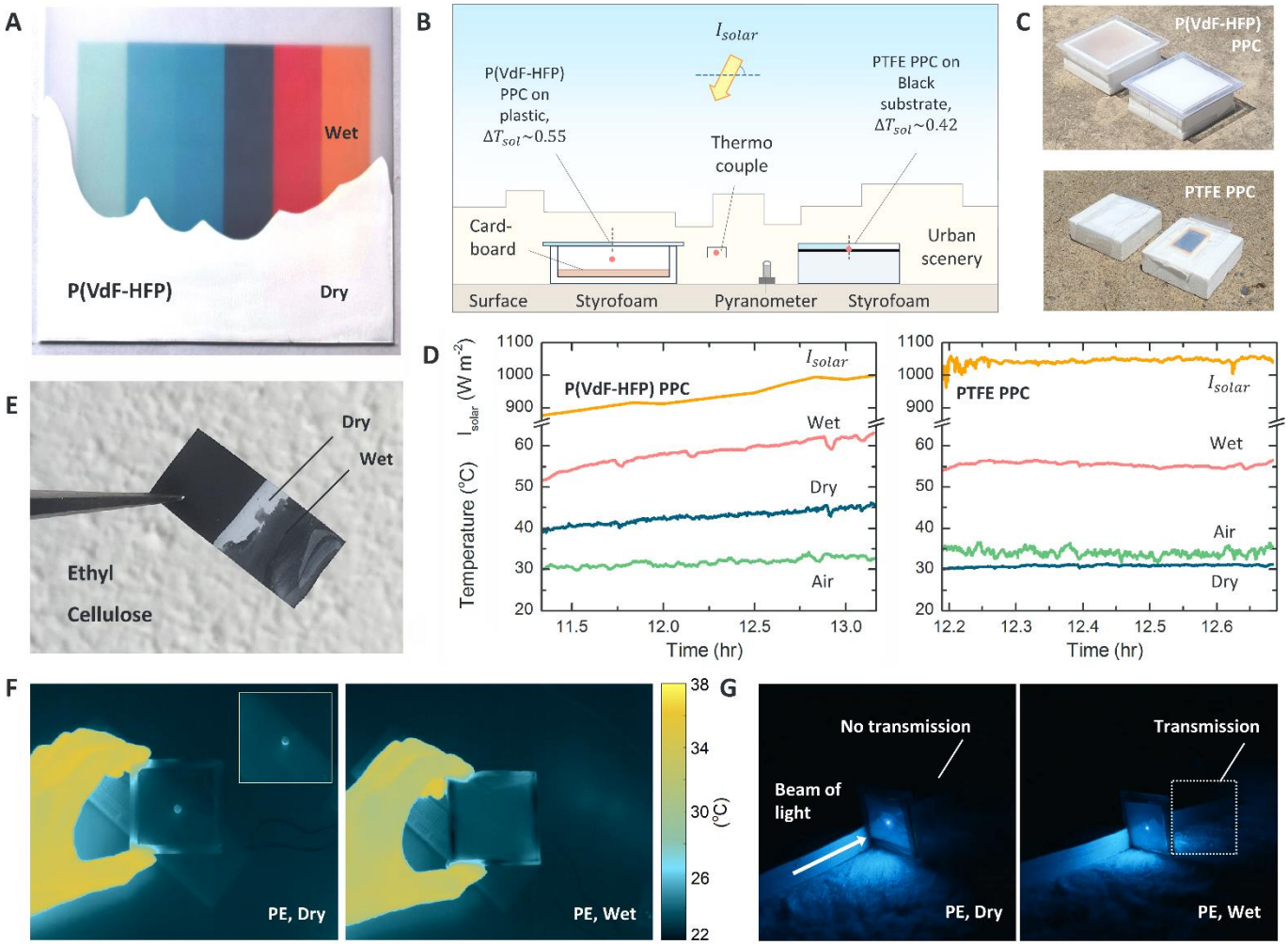

Figure 4. Potential uses of PPC-air/liquid systems. **(A)** P(VdF-HFP) PPCs are a color-neutral platform that can be used to control daylight in buildings. Coupling with colored, dark and light backgrounds can enable controlled cooling or heating. **(B)** Schematic of P(VdF-HFP)-air/isopropanol and PTFE-air/isopropanol systems as roofs on miniature houses. The first switches between solar reflective and transparent states, and the second switches between solar reflective and absorptive states. **(C)** Photographs of the two setups. **(D)** Under strong sunlight, the wet and dry roofs lead to significantly different temperatures. For the P(VdF-HFP) air/isopropanol systems, indoor temperature differences ~18˚C are observed, while for PTFE-air/isopropanol roofs, sub-ambient radiative cooling by 3.2˚C and above-ambient solar heating by 21.4˚C is achieved. **(E)** Hydrophilic PPCs such as porous ethyl cellulose exhibit optical switching with water, which may have additional uses as an adaptive paint responsive to rain or snow. **(F)** Dry icehouse and wet greenhouse states of the porous PE-air/alcohol system shown in the LWIR and **(G)** the visible wavelengths. Inset in (F) shows the warm light-emitting-diode without the switchable transmitter in front.

One of the most promising applications of PPCs is the control of daylight and heat in buildings, which accounts for more than 30% of building energy usage and is a major architectural challenge.[18–22] P(VdF-HFP) PPCs, which attain a ΔT_{vis} (~ 0.80), can greatly modulate daylight in buildings to reduce lighting and shading costs (Fig. 4A), and potentially be used in switchable displays (Fig. S7). On the other hand, the large ΔT_{sol} of P(VdF-HFP) PPCs is useful for thermoregulation. To demonstrate this, we placed dry and wet P(VdF-HFP)-air/isopropanol systems ($\Delta T_{sol} \sim 0.55$) as roofs on two miniature houses (Figs. 4B and 4C upper panel). To represent a practical scenario, wood-colored interiors for the houses, an urban environment with tall buildings nearby, and a translucent rather than a transparent wet roof were chosen. As shown in Fig. 4D, under a mid-day summertime I_{solar} of ~ 940 W m^{-2}, the 'indoors' of the houses became ~12˚C (white, dry) and ~30˚C

(translucent, wet) warmer than the ambient air (at ~ 30˚C). The performance can be pushed even further to yield switchability between sub-ambient radiative cooling and solar heating functionalities. We demonstrate this using PTFE PPCs – which have high reflectance R_{sol}~ 0.95 (Fig. S4) and yield ΔT_{sol}~0.42 upon wetting with isopropanol – as switchable roofs. When coupled with 'black roofs' on Styrofoam blocks (Figs. 4B and 4C lower panel), they can achieve sub-ambient passive daytime radiative cooling by ~ 3.3˚C for the dry state and above-ambient solar heating by ~ 21.4˚C for the wet state (Fig. 4D). The sub-ambient cooling, obtained under a solar intensity of 1043 Wm^{-2} and in an urban environment with limited exposure to the sky, is on par with notable radiative cooling designs in the literature,[1,6,23–26] and together with the solar heating functionality, is perhaps unprecedented.

The dynamic thermoregulation capability makes PPC-based switchable devices attractive for use in buildings, vehicles and water-tanks (Fig. S8 and S9) in varying diurnal or seasonal environments. Furthermore, unlike electrochromic and thermochromic systems, the PPCs are color neutral (Fig. 4A), and reflective rather than absorptive when opaque. The first overcomes the longstanding problem of tinting in smart windows, while the second ensures that the solar-blocking 'cool' state does not itself become hot under sunlight. Similar optical switching can be achieved with hydrophilic PPCs that are compatible with water. Ethyl-cellulose-air/water systems (Fig. 4E), for instance, can achieve large ΔT_{sol}~0.40 (Fig. S4), and could be used as an alternative to alcohol-based systems in adaptive panels (Fig. 3A) or in optical water-sensing applications. Additionally, hydrophilic PPCs could also be used as adaptive exterior paint coatings that switch in response to precipitation – such coatings could passively heat or cool buildings depending on the season in regions with dry summers and wet winters.[27]

While P(VdF-HFP), PTFE and ethyl-cellulose PPCs exhibit a large ΔT_{sol} and ΔT_{vis} , the PE-air/alcohol system can modulate both solar and thermal transmissions by switching between icehouse and greenhouse states (Figs. 1D-F, 4F-G). The simultaneous $\Delta T_{sol} \sim 0.33$ and $\Delta T_{LWIR} \sim -0.64$ can enable a solar modulation exceeding 350 W m^{-2}, and a modulable heat emission through the LWIR atmospheric window exceeding 70 W m^{-2} (Table S3). Consequently, PE-air/alcohol systems can be used for both daytime and nighttime thermal management. Furthermore, by pairing with metal backings, switching from IR-reflective (i.e. non-emissive) to emissive states can be achieved.

Table 1. Comparison of PPC-based switchable optical devices with other switching paradigms. Values marked with (*) are likely specular (normal-normal) ΔTs which may be higher than corresponding diffuse values. The value marked with (†) is an estimate based on extrapolation of available data. Calculations of the relative efficiencies are presented in Section 13 of the Supplemental Information.

Property	Electrochromic[13,30]	Electrodeposition[36]	Thermodynamic[32]	Thermochromic[13,34]	Liquid Crystal[13,38]	Porous Polymer Coating
ΔT_{sol} / ΔT_{Vis}	0.68 / 0.74	0.60† / 0.75	0.40* / 0.66*	0.19 / 0.47	0.51* / 0.56*	**0.74 / 0.80**
Transition type	Absorptive /Colored to transparent	Absorptive /Dark to transparent	Reflective /White to transparent	Absorptive /Colored to transparent	Reflective /White to transparent	**Reflective/White to transparent**
Transition Point	n/a	n/a	Fixed Temperature (θ)	Fixed Temperature (θ)	n/a	**n/a**
Switching Speed	< 60s	< 60s	Minutes, ∝ dθ/dt	Minutes, ∝ dθ/dt	< 5s	**< 60s**
Spectral range	Solar, MWIR, LWIR	Solar	Solar	Solar, MWIR	Solar	**Solar, MWIR, LWIR**
Relative Efficiency	≲1	≲1	n/a	n/a	≪1	**1**

The PE-air/alcohol system may also have applications in thermal camouflage.[3,28] As shown in Figs. 1D and 4F, because of its high LWIR transparency when dry, it transmits thermal signatures from underlying objects. However, when wet, the now-absorptive system cloaks underlying objects and shows its LWIR temperature instead. By appropriately choosing alcohols[29] and heating or cooling them, the LWIR temperature of the system can be set between -110˚C (the freezing point of ethanol) and 110 ˚C (melting point of polyethylene) to blend in with the environment, and across a wider temperature range than possible with most electrochromic designs.[3,12,14]

Lastly, we present our PPC-based switchable optical devices in context of notable optical switching paradigms. As shown in Table 1, the ΔT_{sol}/ ΔT_{vis} up to 0.74/0.80 achievable with PPCs is better than or on par with those of notable electrochromic,[3,8–10,12,30] thermodynamic,[31,32] thermochromic,[13,33–35] electrodeposition-based[36] and liquid crystal-based[13,37,38] designs. Unlike electrochromic, thermochromic or electrodeposition-based systems, PPCs described here have no intrinsically solar absorptive states and are also color neutral, and unlike thermodynamic or thermochromic systems, which switch at set temperatures,[13,31,32,34] they can be switched at will. Although slower than liquid crystal-based designs, PPCs exhibit a comparable switching speed to electrochromic and electrodeposition-based designs, and are faster than thermochromic and thermodynamic systems.[13,30–32,34,36] Furthermore, PPCs may require less switching energy than electrochromic, electrodeposition-based or liquid crystal-based designs (Supplemental Information, Section 13). And because they can be easily created using simple materials, they are promising for widespread manufacturing and use. With appropriate fluid pumping and collection systems, PPCs with switchable optical transmittance could be scaled to large installations. Given these aspects, they are a potentially affordable and energy-efficient paradigm for high performance optical and thermal management, and a promising alternative to more sophisticated switching paradigms.

Experimental Procedures

Fabrication of porous polymer coatings and devices: P(VdF-HFP) PPCs were coated using a previously demonstrated phase inversion technique[1] onto acrylic substrates, which were then assembled into devices. P(VdF-HFP) (Kynar Flex 2801) from Arkema was used. Ethyl-cellulose PPCs were similarly coated on black foils. PTFE PPCs were made from commercially available thick 'Teflon tape'. PE PPCs were made by hot-pressing multiple layers of commercially available battery separators to get the desired thickness. The PE PPCs were then inserted into enclosures consisting of 25 μm PE films and plastic side-frames.

Optical Characterizations: Spectral transmittance of the PPCs was determined separately in the visible to near-infrared (0.40-1.05 μm) and near-infrared to mid-infrared (from 1.06 up to 14 μm) wavelength ranges. For the first range, measurement was taken at specific wavelengths from a high-power supercontinuum laser (SuperK Extreme, NKT Photonics) coupled to a tunable filter (Fianium LLTF contrast) and an integrating sphere (Model IS200, Thorlabs). For the second range, a Fourier Transform Infrared (FT-IR) spectrometer (Vertex 70v, Bruker) and a gold integrating sphere (Model 4P-GPS-020-SL, Labsphere), along with a mercury cadmium telluride detector were similarly used. Samples were placed at the entrance of the integrating spheres, with the beam shining onto the integrating spheres at normal incidence. Measurement of the unobstructed beam was used as a reference. The spectra were then used to calculate the integrated transmittances T_{sol} , T_{vis} , and T_{LWIR} by weighted integration using normalized ASTM G173 Solar Spectrum or the blackbody spectrum at 25˚C.[1]

Imaging and microscopy: Images of samples were taken using Nikon D3300 (visible) and FLIR T640 (LWIR) cameras. Scanning electron microscopy was done using a Zeiss Sigma VP scanning electron microscope.

Scattering Cross-Section and Transmittance Calculations: Scattering cross sections were simulated using FDTD Solutions 8.6.1 software by Lumerical. Predicted transmittance of the PE-air/alcohol system were calculated using a multilayer model of the structure in Fig. 2F. Because of the varying thicknesses of PE PPCs and the enclosing PE films across their areas, optical interferences arising from multiple reflections averaged to zero. Furthermore, because reflectivity coefficients at the multilayer boundaries were low (< 0.04) multiple reflection effects were not significant. Therefore, the transmittance of the PE-air/alcohol system was simply calculated as the product of the transmittance at each interface of the multilayer and the optical attenuation in between. For the calculations, spectral refractive indices of P(VdF-HFP) and alcohols were obtained from the literature,[1,39] and that of PE was calculated from spectral transmittances of films with different thicknesses. For PE PPCs having 40% porosity, effective refractive indices were calculated using the Bruggeman model.

PPC-air/fluid system operation: The devices represented by Fig. 3A were wetted by flowing isopropanol into the enclosure through the pipes, and dried by blowing air or nitrogen.

Thermoregulation experiments: For the first experiment, two miniature houses, with Styrofoam walls and floors and a cardboard 'carpet' on the floor were made, and had P(VdF-HFP)-air/isopropanol systems, one wet and one dry, placed on them as roofs. Thermocouples tipped with white paper were placed to record the 'indoor air temperature', and the ambient temperature outside. The houses were then left in an urban setting under the sun (Date: 2018-07-11, location 40.810˚N, 73.961˚W) and had their temperatures measured. For the second experiment, a simple PTFE-air/isopropanol system was used. PTFE PPCs were attached to black painted aluminium sheets, which themselves were attached to the insides of thick polyethylene zip-lock bags. The sides of the bags in contact with the aluminium were attached to thermocouples. The systems were then placed on polystyrene blocks under sunlight in an urban setting (Date: 2019-05-26, Location: 40.806˚N, 73.959˚W). In both cases, solar intensity was measured using a pyranometer (Apogee, SP 510).

Acknowledgments

This work was supported by startup funding from Columbia University, AFOSR (Y.Y. grant no. FA9550-18-1-0410), AFOSR MURI (Multidisciplinary University Research Initiative) program (N.Y. grant no. FA9550-14-1-0389), AFOSR DURIP (Defense University Research Instrumentation Program) (N.Y. grant no. FA9550-16-1-0322), and the National Science Foundation (N.Y. grant no. ECCS-1307948). J.M. acknowledges support from the Schmidt Science Fellows Program, in partnership with the Rhodes Trust.

Author contributions: J.M. discovered the switchable solar transmittance of P(VdF-HFP) PPCs, extended the concept to PTFE and ethyl-cellulose, and conceived and demonstrated switchability in thermal infrared wavelengths. J.M. and Y.Y. conceived applications and designed the experiments. J.M. conceived the design of PPC-air/liquid systems and chose polymer-liquid combinations. J.M. performed the simulations and theoretical calculations. M.J., J.M. Y.F. and E.C. designed the PPC-air/liquid systems. J.M. and A.O. performed the optical measurements. J.M., Y.Y., N.Y. and A.O. wrote the manuscript.

Declaration of Interests: A provisional patent (U.S. 62/596,145) has been filed related to this work.

Data and materials availability: All data are available in the manuscript or the supplementary materials. Information requests should be directed to the corresponding author.

Supplemental Video Titles

Video 1 – Optical switching of a P(VdF-HFP) PPC

Video 2 – Device with high-speed switching

Video 3 – A potential device design

Video 4 – Non-flammability of a 2:1 mixture of Water and Isopropanol

(Please check https://doi.org/10.1016/j.joule.2019.09.016 for the videos)

Accepted Manuscript of Mandal et. al. *Joule,* 3(1-12) DOI: 10.1016/j.joule.2019.09.016.

Supplemental Information

Porous Polymers with Switchable Transmittance for Optical and Thermal Regulation

Jyotirmoy Mandal,[1] Mingxin Jia,[2] Adam Overvig,[1] Yanke Fu,[1] Eric Che,[3] Nanfang Yu,[1] Yuan Yang*[1]

[1] Department of Applied Physics and Applied Mathematics, Columbia University, New York, NY, USA

[2] Department of Mechanical Engineering, Columbia University, New York, NY, USA

[3] Hunter College, City University of New York, New York, NY, USA

Section 1: The LWIR Switching of Poly(ethylene) PPCs

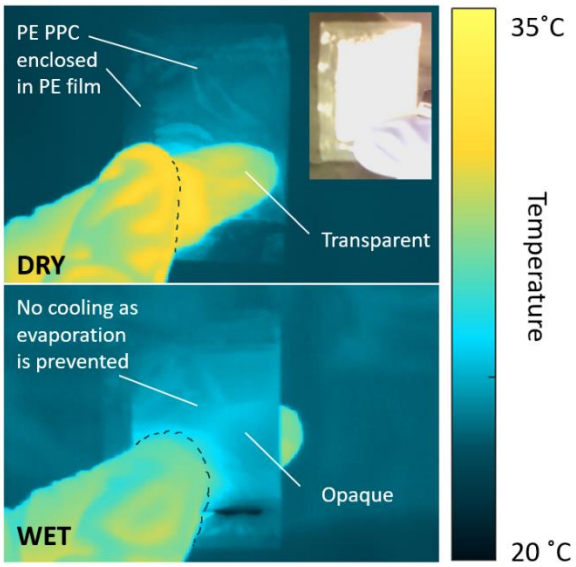

Figure S1. Annotated version of the LWIR thermographs Fig. 1E, with color bar and a photograph of the PE-air/isopropanol device in the inset. The solid, LWIR transparent poly(ethylene) film enclosing the PPC is more starkly visible in the photograph.

Section 2: The effect of Δn on Visible/Solar Transmittance

Fig. S2 shows a 100 μm thick polyethylene PPC held against a light source in the background. As evident, as the refractive index of the fluid in the pores approaches that of polyethylene, the optical transparency increases from opaque (in case of air) to translucent (in case of isopropanol) to nearly transparent (in case of oil). Almost perfect transparency can be achieved using index-matched liquids, but to achieve a balance between performance, simplicity and cost, we limit ourselves to commonly available fluids.

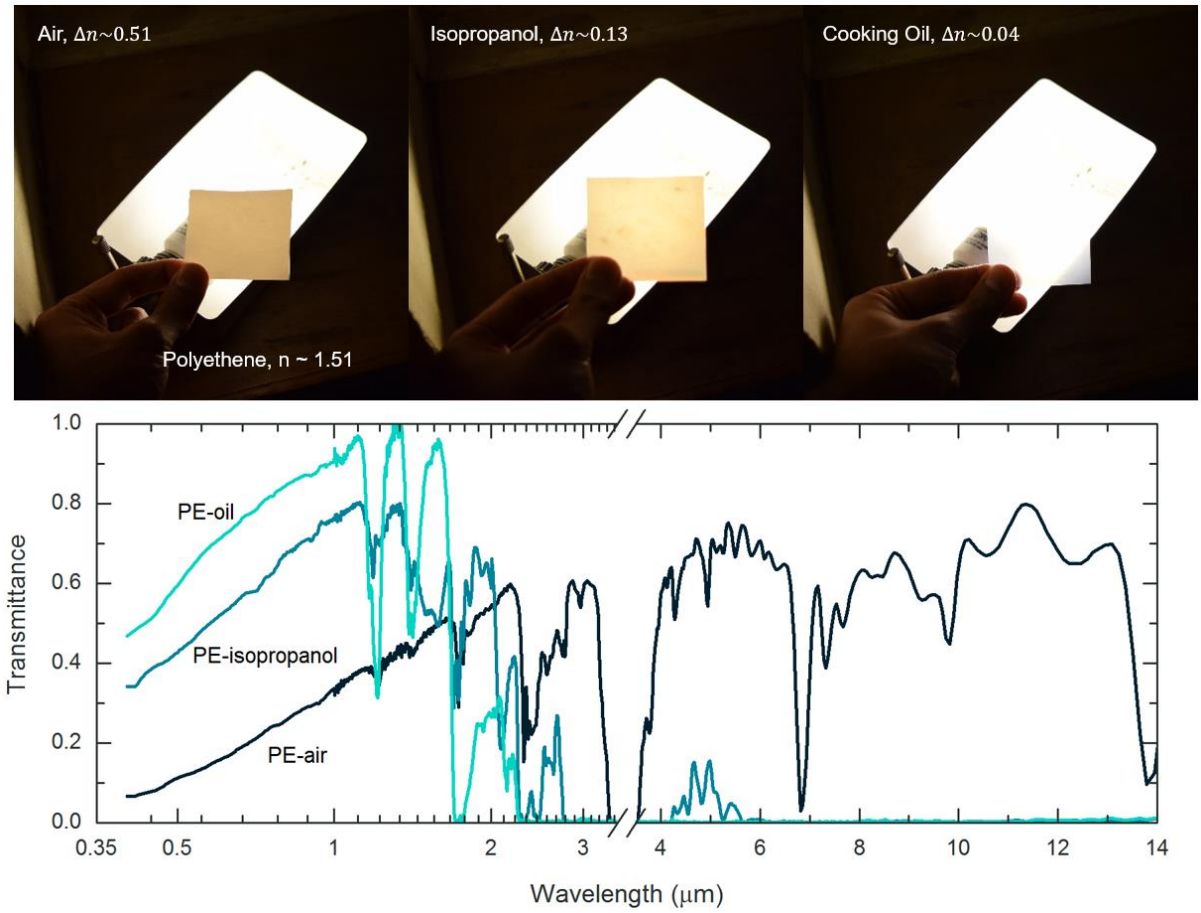

Figure S2. (Top) Left to right: transmittance of Polyethylene PPC when dry ($\Delta n \sim 0.51$), wet with alcohol ($\Delta n \sim 0.13$) and wet with vegetable oil ($\Delta n \sim 0.04$). Transmissive samples let light through and appear brighter. The yellowish appearance indicates higher scattering of shorter wavelengths in the visible. (bottom) Spectral transmittance of PE-air/isopropanol/cooking oil systems. As evident, a lower Δn results in a higher solar transmittance, with a ΔT_{sol} of 0.51 achieved with cooking oil, compared to 0.33 achieved with isopropanol.

Section 3: The Effect of Thickness on the Performance of Porous Polyethylene-based Switchable Optical Devices

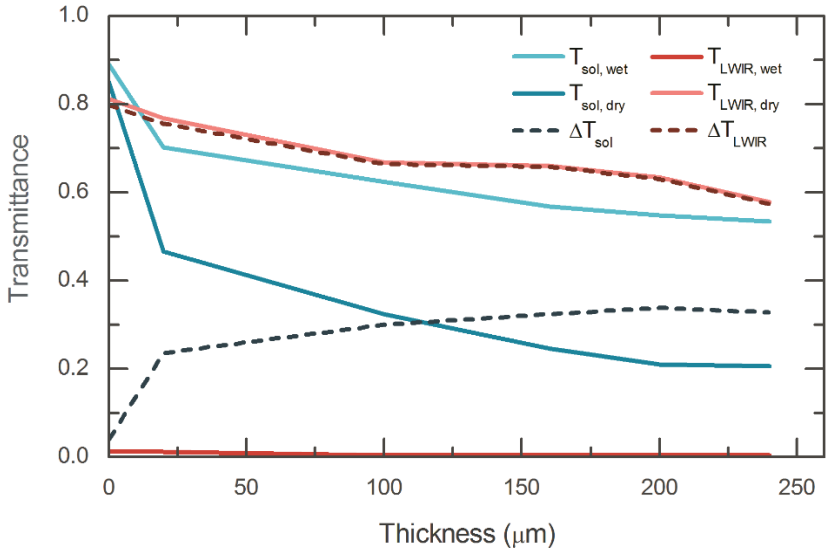

Figure S3. The effect of thickness of PE PPCs on the diffuse transmittance of PE-air/alcohol system, comprising of the PPCs enclosed by 25 μm PE sheets. As shown, ΔT_{LWIR}~ 0.66 for a thickness of 100-150 μm, and ΔT_{sol} peaks at 0.34 for a thickness of 200 μm. For smaller PE PPC thicknesses, the decreasing intrinsic LWIR absorption of the dry state means that the relative increase due to wetting is more, causing ΔT_{LWIR} to rise. However, ΔT_{sol} drops as the already low scattering by thinner PPCs cannot be significantly lowered by wetting. A ~160 μm thick PE PPC, on the other hand, achieves both high ΔT_{sol} and ΔT_{LWIR}.

Section 4: Optical Switching of a Porous PTFE-air/isopropanol system and a porous Ethyl-Cellulose-air/water system

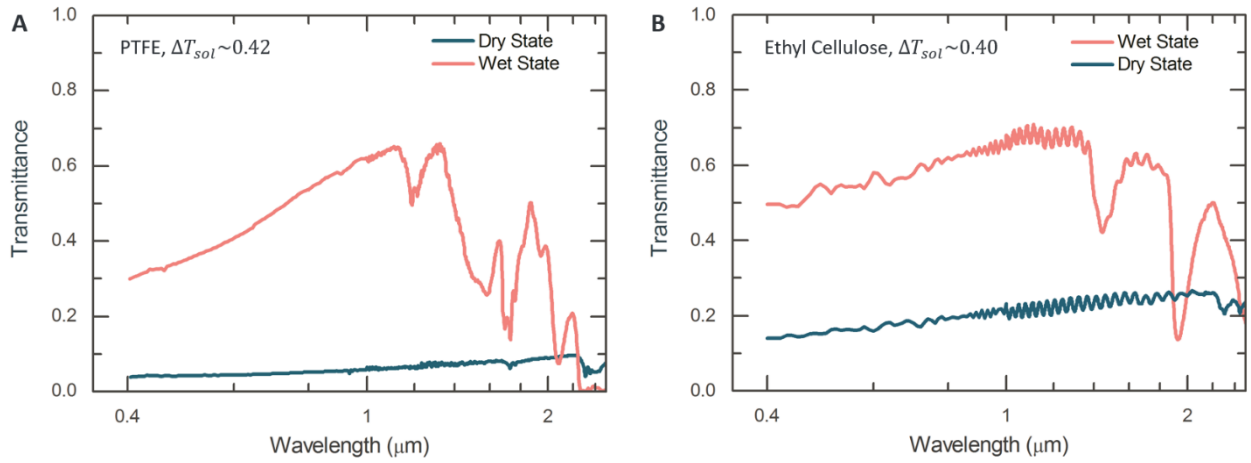

Figure S4. (A) Spectral transmittance of PTFE (n~1.36) PPCs with thicknesses ~ 0.5 mm when dry or wet with isopropanol (n~1.38). Evidently, dry PTFE PPCs have a high solar reflectance (>0.95), as evidenced by the transmittance of the dry state. ΔT_{sol} is calculated to be 0.42. **(B)** Spectral transmittance of the dry and wet states of an ethyl cellulose (n~1.49) PPC with thickness ~ 100 μm. The ΔT_{sol}, which is brought about by wetting with water (n~1.33), is ~ 0.40.

Section 5: Device Design – Enabling Fast Switching Speed

While the 150 mm x 150 mm PPC based device in Fig. 3A can achieve a fast, sub-minute switching speed, the switching time for PPCs can vary depending on factors such as the speed of air flow, wettability of liquid and device design. One potential issue is that during drying, air flowing in the device might become saturated with vapor and slow the drying process. Here, we suggest two strategies that can address the issue and enable fast switching.

The first is widening the air gap inside the device to provide a large cross-sectional area for air flow. This has two advantages:

1. This allows for greater volume of air to flow and mix during drying, reducing the chance of saturation of downstream air in the device with vapor. Consequently, the PPC can dry faster.
2. Given the nature of laminar air flow, for a wider cross-section area, air near the center experiences lesser drag from the boundaries compared to what it experiences for a smaller area of flow. Therefore, the air flow per unit area is faster, allowing for quicker drying.

The second is the use of a modular design, where smaller modules are used instead of a large device (Fig. S5). Each module has its own air/liquid flows. Consequently:

1. The air flow path of each segment is short, so the likelihood of saturation of air with vapor downstream is reduced, enabling a faster switching.
2. More, dry air (or liquid) can be fed into the device due to inlets/outlets at frequent spatial intervals compared to a single large device, which only has inlets/outlets at the ends.

These strategies can be combined with other modifications, such as coating both inner faces of the enclosure with thinner PPCs rather than having a thick PPC on one side (therefore doubling the surface area for wetting and drying), to create fast switching devices.

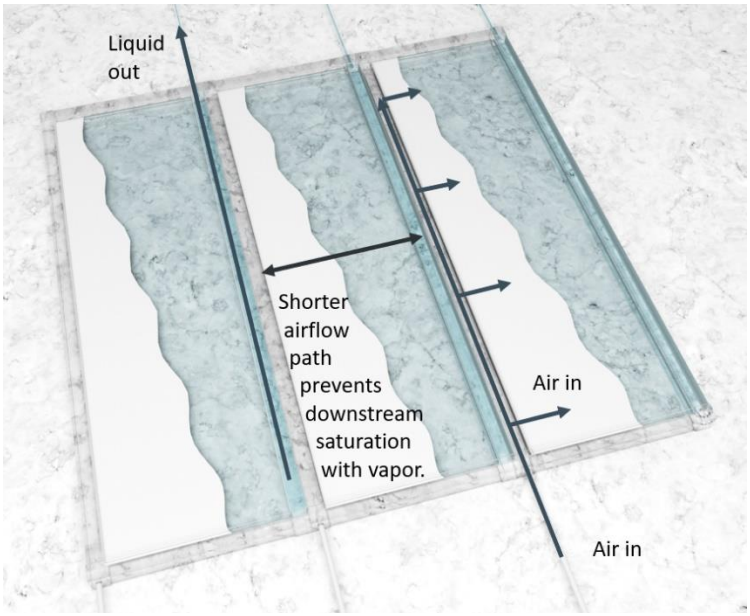

Figure S5. A modular device design shown during the drying process. It enables faster switching by reducing the air flow path length, and increasing the number of inlets/outlets.

Section 6: Device Design – Reducing Flammability and Environmental Impact

Although alcohols like ethanol and isopropanol provide an excellent refractive index match with polymers like P(VdF-HFP) and PTFE, their flammability and environmental impact may pose a safety risk. However, fire hazards can be reduced or even eliminated, and the environmental impact minimized, by greatly diluting the alcohol with water. For instance, a mixture of isopropanol and water in a 1:2 mass ratio does not catch fire (Video S4), and can wet and switch the transmittance of porous P(VdF-HFP) by 0.53 (from 0.11 for the dry state to 0.64 for the wet state) (Fig. S6). Although lower than the ΔT_{sol} (0.67) achieved with isopropanol, the transmittance switching with the alcohol-water mixture is still 80% of the former, and comparable to notable electrochromic and thermochromic designs (Table 1).

Fire and environmental hazards can also be eliminated if hydrophilic PPCs that switch upon wetting with water are used. Ethyl cellulose-air/water systems, for instance, exhibit a large ΔT_{sol}~ 0.4 (Fig. S4). Polymers (e.g. P(VdF-HFP), n~ 1.40) which have a closer refractive index to that of water (n~1.33) could also potentially be chemically treated to make them hydrophilic,[40,41] and yield higher ΔT_{sol}. Although the high freezing point of water (0˚C) limits operation at extremely low temperatures, the addition of common anti-freezing agents like ethylene glycol and alcohols can enable the use of water-based systems at temperatures of -20˚C or lower.

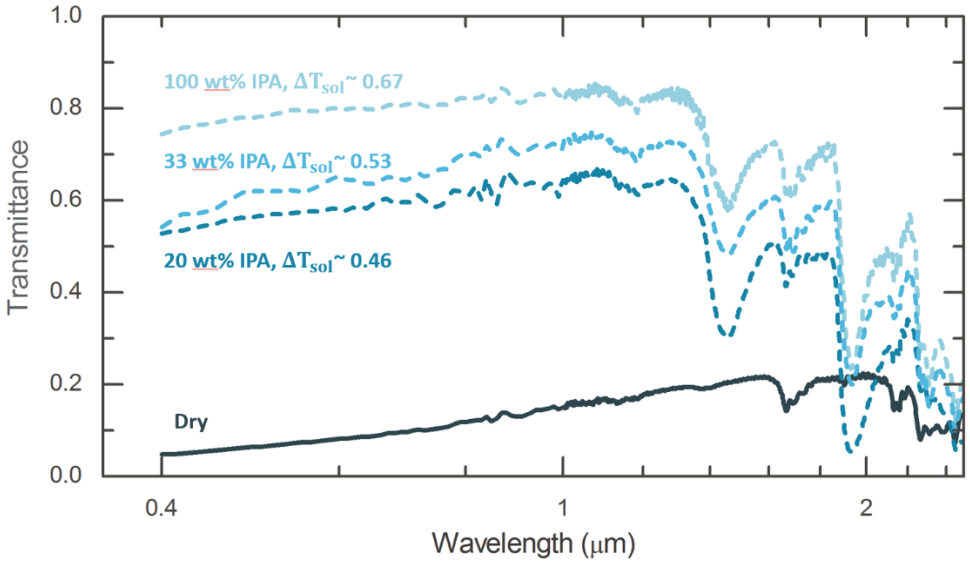

Figure S6. Transmittance spectra showing the optical switching of P(VdF-HFP)-air/liquid systems with different mixtures of water and isopropanol used as the wetting liquid. With increasing water content, ΔT_{sol} decreases because of the larger Δn for the wet state. However, the ΔT_{sol} values are still high (0.53 and 0.46 for the 33 wt% and 20 wt% IPA mixtures respectively, compared to 0.67 for pure IPA), and importantly, obtained with liquids that do not catch fire.

It is noteworthy that in cases where the optical performance and fast switching of the P(VdF-HFP)-air/alcohol systems are indispensable, the device in Fig. 3A can be engineered to minimize fire and environmental hazards. For instance, flame retardants could be added to the alcohol and the device itself to reduce flammability. Using modular designs (Fig. S5) and narrower enclosure gaps (Fig. 3A) would also reduce the amount of combustible alcohol in case of leaks, while the use of gaseous nitrogen rather than air in the enclosure may also reduce fire hazards within the device. Lastly, safety controls, such as chemical and temperature resistant seals to prevent alcohol leakage, would reduce environmental risks as well.

Section 7: Stability of Porous Polymer Coatings

For long-term use in PPC-air/liquid systems, porous polymer coatings should be stable when subject to operational stresses such as solar exposure, high temperatures and wetting with liquids. To test for the stability of PPCs in such conditions, we performed a series of tests on bare P(VdF-HFP) and PE PPCs, following which they were integrated into PPC-air/liquid systems and had transmittance measurements taken. Measurements were also performed for control samples that were kept pristine. Details of the tests, and the results are presented in Table S1. Some of the stability test results for P(VdF-HFP) (marked with *) are quoted from our previous study on P(VdF-HFP) PPCs.[1]

Table S1. Results of the stability tests conducted on P(VdF-HFP) and PE PPCs. Tests marked with * and the corresponding solar reflectances (R_{sol}) are quoted from a previous study.[1]

Polymer	Test	$T_{sol,wet}/T_{sol,dry}$ or R_{sol}*	
		Pristine	After Test
P(VdF-HFP)	Heating at 60˚C in isopropanol for 8 days	0.77/0.13	0.76/0.12
	Heating at 80˚C in air for 14 days*	0.95	0.95
	Heating at 80˚C in 100% relative humidity for 14 days*	0.96	0.93
	Outdoor exposure for a month in New York City in winter*	0.94	0.93
	Outdoor exposure for 8 days in New York City in summer*	0.99	0.99
		$T_{sol,wet}/T_{sol,dry}$ & $T_{LWIR,wet}/T_{LWIR,dry}$	
Polyethylene	Heating at 60˚C in air for 8 days	0.49/0.17 & 0.0/0.62	0.49/0.16 & 0.0/0.65
	Heating at 60˚C in isopropanol for 8 days		0.51/0.17 & 0.0/0.63
	Outdoor exposure for 8 days in New York City in summer.	0.51/0.20 & 0.0/0.68	0.51/0.20 & 0.0/0.70

It is evident from the results in Table S1 that the performance of the P(VdF-HFP) and PE PPCs are essentially unchanged after the stability tests. In fact, in some cases, such as T_{LWIR} of the PE PPCs, the performance seems to slightly improve after the stability tests. Considering that the tests involved harsh working conditions such as temperatures of 60-80˚C, exposure to liquids like isopropanol or water, and summertime outdoor solar exposure, the observed stabilities of the PPCs are promising for applications. Furthermore, P(VdF-HFP) and PE separators are also known to be mechanically stable.[1,42] In real-life scenarios, they would also be protected by their enclosures (Fig. 3A), which can be made from mechanically strong plastics, glasses or thick polyethylene sheets[43] as appropriate to offer further stability.

We finally note that given the diversity of polymers, PPCs with high stabilities for solar and thermal management applications are available. For instance, fluoropolymers such as P(VdF-HFP), PVdF and PTFE are used in exterior coatings on buildings for their resistance to common chemicals and durability under sunlight.[44,45] High density polyethylene, from which the PE PPCs in this study are fabricated, is inert to typical alcohols and after treatment with UV stabilizers, can be used as greenhouse covers that are stable under sunlight.[43] Based on these findings, we conclude that PPC-based switchable transmitter designs are suitable for outdoor use.

Section 8: Schematic of a Switchable Display Device

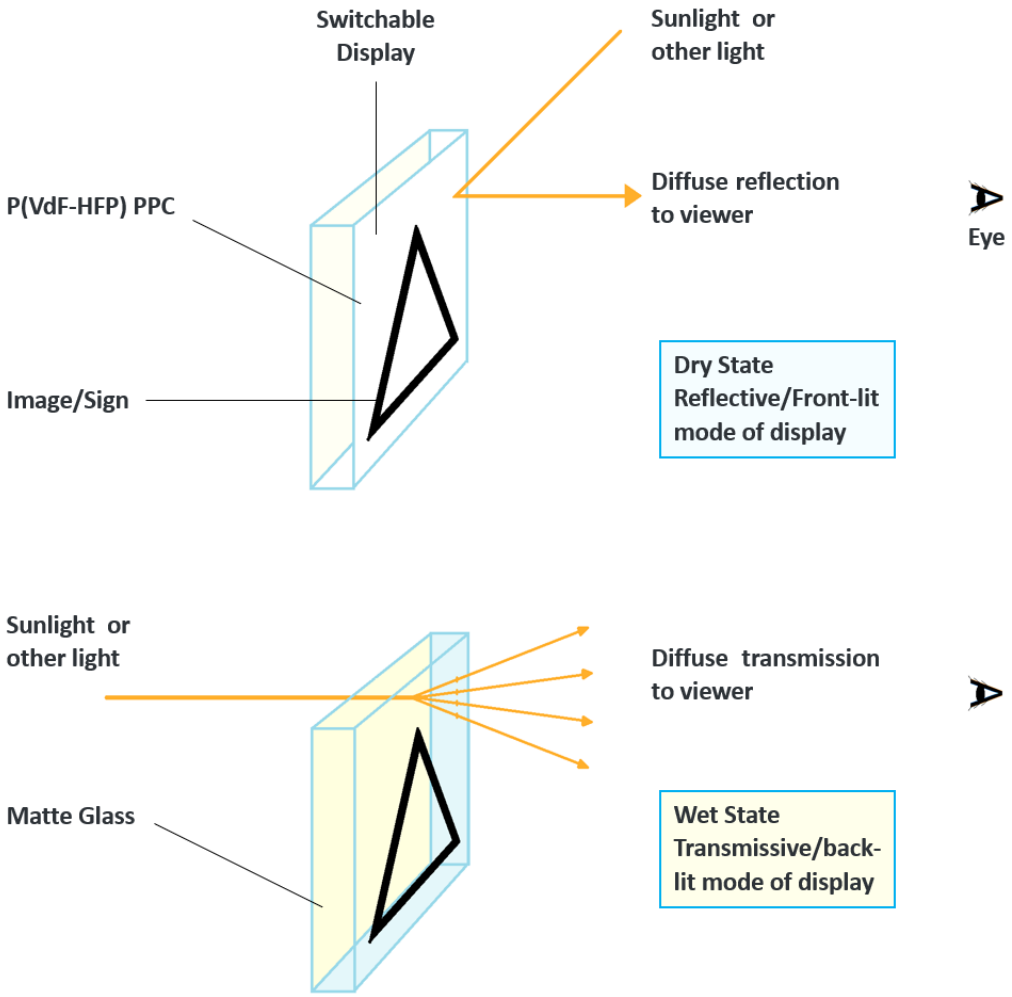

Figure S7. Schematic of a switchable display, based on a PPC that switches between front-lit and back-lit modes. This could potentially be used in road-signs or advertising displays depending on solar position or time of day/night.

Section 9: Schematic of a Switchable Water Heating/Cooling Device Using a Porous Polymer Coating

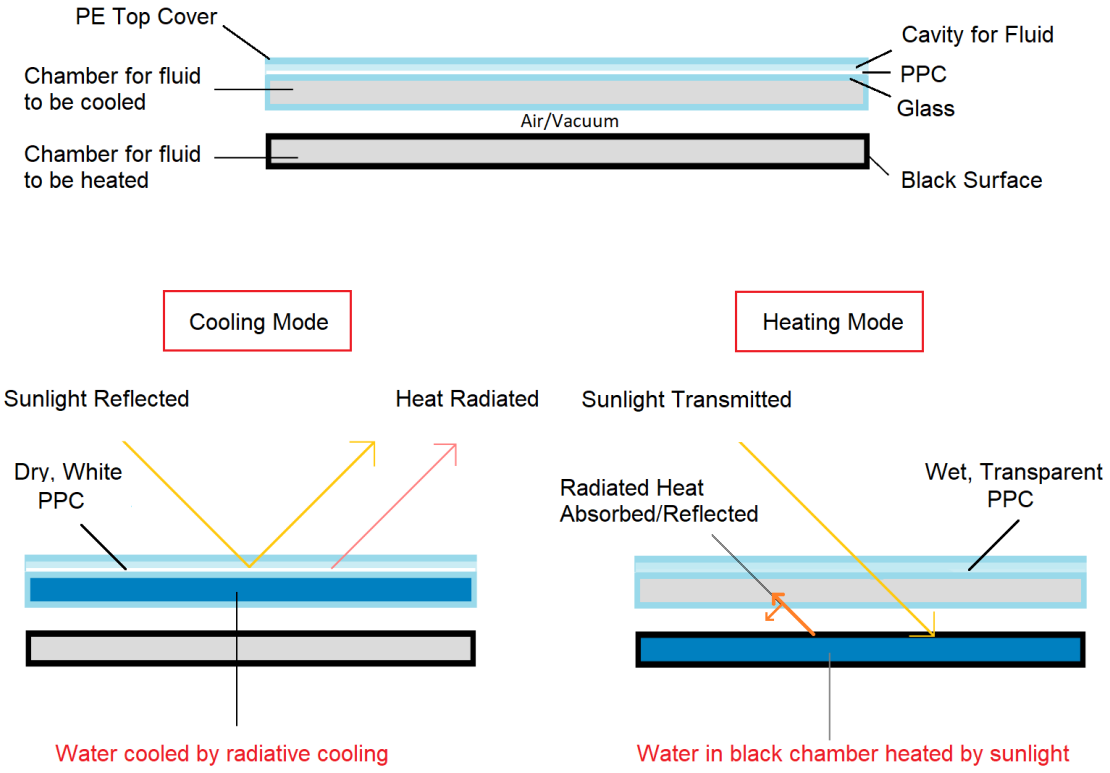

Figure S8. Schematic of a device, based on a PPC that can switch between cooling and heating modes for water. This can be used for heating or cooling water, or buildings themselves.

Section 10: Types of Porous Polymer Coatings and Their Suitability for Transmittance Switching

The table below presents a variety of porous polymer coatings that could potentially be used as switchable solar (and in some cases, thermal) transmitters. While some examples, such as P(VdF-HFP) are high-performance and are perhaps first reported in this work, some, like paper (which turns appreciably transmissive when wetted with water), are more common examples.

Table S2. Examples of porous polymers, their fabrication and availability, compatible liquids for optical switching and advantages.

Porous Polymer	Fabrication/availability	Suitable Liquids	Advantages
P(VdF-HFP)	Phase inversion[1]	Alcohols, alcohol-water mixture	High ΔT_{sol}
PVdF	Phase inversion[1]	Alcohols, alcohol-water mixture	High ΔT_{sol}
Poly(tetrafluoroethene)	Commercial membrane	Alcohols, alcohol-water mixture	High ΔT_{sol}
Polyethylene	Commercial membrane	Alcohols, alcohol-water mixture	ΔT_{sol} and ΔT_{LWIR}
Poly(propylene)	Commercial membrane	Alcohols, alcohol-water mixture	ΔT_{sol} and $\Delta T_{LWIR}{}^{4}$
Nylon	Commercial fabric	Alcohol, water	ΔT_{sol} and $\Delta T_{LWIR}{}^{4}$, water compatible
Poly(methyl methacrylate)	Phase inversion[1]	Alcohols, water	Water compatible
Paper (cellulose)	Commercial	Alcohol, water	Water compatible
Ethyl Cellulose	Phase inversion[1]	Water	Water compatible
Poly(ethene terephthalate)	Commercial fabric	Alcohols, alcohol-water mixture	

Section 11: Effect of Wind on Thermoregulation Performance of a PPC-based White/Black Switchable Rooftop Device

In this section, we present the expected temperature difference between the white and black states of large switchable rooftop devices (Fig. 4B, PTFE PPC, ΔT_{sol}~ 0.42) assuming a solar intensity of 1100 Wm^{-2} (urban summer noon, with sunlight reflected from nearby buildings and objects) and warm ambient temperatures ~ 30˚C under various wind-speeds. The conduction by the Styrofoam is considered to be negligible, and the devices are approximated to be large enough that edge effects are minimal. Convection coefficients corresponding to various wind speeds are used to calculate the difference between steady state temperatures of white and black states subject to convective and radiative heat transfer.

The results are shown in Fig. S9. Evidently, under windless conditions (0-1 m s^{-1}) experienced by buildings and stationary vehicles, the temperature difference is quite large, about 35-40˚C. The ~25˚C temperature difference observed in Fig. 4D under an I_{sol}~1043 Wm^{-2} is consistent with the convection coefficient (10 $Wm^{-2}K^{-1}$) expected for mild breezes (~ 2 ms^{-1}) occurring during the experiments. Even for large wind speeds that moving cars might experience (20 ms^{-1} or 72 km h^{-1}, corresponding to a convection coefficient of 76 W m^{-2} K^{-1}), the temperature difference is still an appreciable 6˚C. Clearly, the devices can exhibit an appreciable control of temperature even under windy conditions.

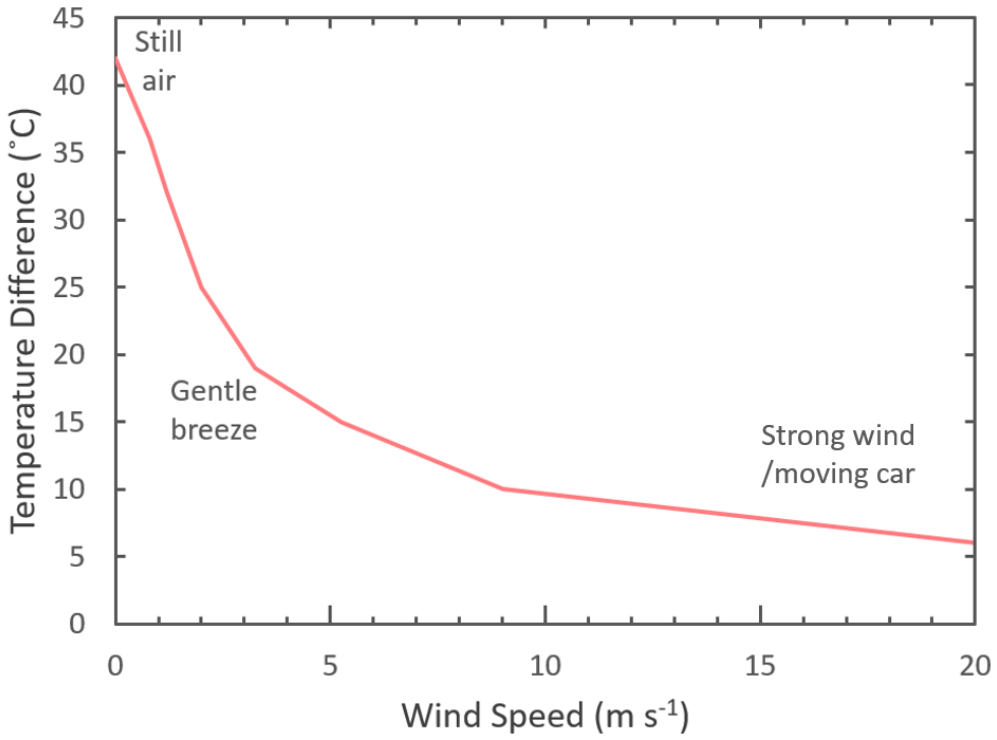

Figure S9. Expected steady-state temperature difference between the black and white states of the PTFE-air/isopropanol system (Fig. 4B) under various wind speeds.

Section 12: Simple Calculation of LWIR Transmission through PE-air/alcohol systems

In this section, we present a simple estimate of the LWIR radiative heat transfer to the sky that can occur through a PE-air/alcohol system from a blackbody on the ground. On a clear, summer day, the LWIR heat loss to the sky from a blackbody at typical ambient temperatures can be ~ 140 W m^{-2}.[1] While most of it occurs towards the zenith rather than the horizon,[46] we first assume that the net radiative heat loss that can occur from the blackbody to the sky is perfectly diffuse.

We then assume that that the PE-air/alcohol system (Fig. 2F) is a flat slab oriented parallel to and above the blackbody, and both are at ambient temperatures. The thicknesses of the PE films (25 μm) and the PE PPC (160 μm) are average values, and 'average out' any optical interference. With these assumptions, and ignoring multiple reflections, we can calculate the transmittance as a function of different incidence angles (Table S3). For the simulated model in Fig. 2F, which has an average transmittance T_{LWIR}~0.65 at normal incidence for the dry state, the angle averaged transmittance (since light incident from the blackbody is equally intense for all angles) is ~0.51 (excluding the transmittance along the horizon as no radiative heat loss can occur there). For a potential radiative heat loss of 140 W m^{-2}, the loss through a dry PE-air/alcohol system is a significant 71 W m^{-2}. As the wet state is completely opaque, this is also equal to the modulable power transmission.

It should be noted that the 71 W m^{-2} value calculated here is a conservative estimate, as the calculation weighs all angles equally. In reality, a majority of the heat loss occurs at low angles,[46] where the transmittance of the dry PE-air/alcohol system is high, so the actual heat loss may be greater.

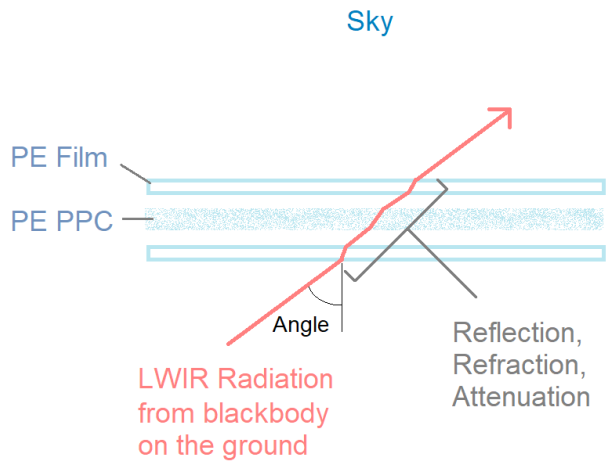

Figure S10. Schematic of a PE-air/alcohol system with transmittance shown at an arbitrary angle.

Table S3. Transmittance through a PE-air/alcohol system for different incidence angles. The average transmittance (excluding the value at 90˚ as no heat loss occurs towards the horizon) is 0.51.

Angle	0˚	10˚	20˚	30˚	40˚	50˚	60˚	70˚	80˚	90˚
T_{LWIR}	0.65	0.64	0.64	0.63	0.61	0.56	0.47	0.31	0.08	0

Section 13: Estimating the Relative Efficiency of the PPC-air/liquid system to those of State-of-the-art Designs

In this section, we estimate a figure of merit indicating the relative performance of the PPC-air/liquid systems and state-of-the-art designs presented in Table 1 of the main text. This figure of merit (η) of a solar transmittance switching design is defined as:

$$\eta = \frac{\Delta T_{sol}}{E},$$

where E is the average energy (of switching in both directions) required to switch the design between states. Besides PPC-based systems, we focus on electrochromic, electrodeposition-based and liquid crystal-based designs, whose energy consumption can be well-quantified. Thermochromic and thermodynamic designs switch spontaneously, hence η is not applicable to those.

To calculate η, we choose a scenario involving a façade of a building that is 10 stories (36m) tall, and is equipped with one of the switchable designs under consideration. We further assume that the designs are ideal, i.e. they have no associated energy (e.g. thermal, overpotential-related) losses.

For the PPC-air/liquid system, we choose a P(VdF-HFP)-air/isopropanol system (Fig. 3A) covering the entire facade, with a 3 mm gap within the enclosure and a ΔT_{sol} of 0.74 (Fig. 3B). We assume that isopropanol is pumped into the device from the bottom to wet the PPC, and conservatively assume that an equally large amount of energy is used for drying the system as well. In that case, the energy required for drying and wetting per square meter area of the device is:

$$E = mg\bar{h} = \rho dg\bar{h} = 786\ kg\ m^{-3} \times 0.003\ m \times 9.807\ ms^{-2} \times 18\ m = 416\ J\ m^{-2}$$

where m is the mass of isopropanol per unit area, ρ is the density of isopropanol, d is the gap within the enclosure, g is the acceleration due to gravity and $\bar{h}$ is the average height of the façade. The figure of merit in that case is:

$$\eta_{PPC} = 1.777 \times 10^{-3}\ J^{-1}m^2.$$

For the electrodeposition-based design, a copper-based device with a ΔT_{sol}~0.6 like that demonstrated by Barile et. al.[36] is assumed. To reversibly electrodeposit an optically thick 200 nm copper layer per square meter, the energy required is:

$$E = VQ = V \times nxF = V \times \frac{d \times \rho}{Molar\ Mass_{Cu}} xF = 0.4V \times \frac{200\ nm \times 8960\ kg\ m^{-3}}{63.5\ g\ mol^{-1}} \times 2 \times 96485\ C\ mol^{-1} = 2178\ J\ m^{-2}.$$

where V is the charging/discharging voltage (assumed to be 0.4 V on average for copper),[36] Q is charge transferred, n is the number of moles of copper per unit area, x is the number of electrons transferred per copper atom, F is the Faraday constant, ρ is the density of copper and d is its thickness. The figure of merit in that case is:

$$\eta_{Electrodep} = 0.275 \times 10^{-3}\ J^{-1}m^2 \text{ or } 0.15\ \eta_{PPC}.$$

Likewise, for the electrochromic design, we consider a design with a ΔT_{sol}~0.68 proposed by Schlotter et. al.[30] which involves a 700 nm thick tungsten oxide (WO_3) layer with reversible intercalation of one lithium ion (Li^+) per WO_3 unit. The switching energy in this case is:

$$E = VQ = V \times nxF = V \times \frac{d \times \rho}{Molar\ Mass_{WO_3}} xF = 0.8V \times \frac{700\ nm \times 7160\ kg\ m^{-3}}{231.8\ g\ mol^{-1}} \times 1 \times 96485\ C\ mol^{-1} = 1669\ J\ m^{-2}.$$

where the variables are defined for WO_3 as for Copper.[30] The figure of merit is:

$$\eta_{Electrochrom} = 0.407 \times 10^{-3}\ J^{-1}m^2 \text{ or } 0.23\ \eta_{PPC}.$$

For liquid crystal-based designs, the case is different in that they do not have a specific switching energy, but require continuous power to maintain a transparent state. In our analysis, we assume the design with ΔT_{sol}~0.51 proposed by

Park et. al.,[38] and conservatively estimate the power consumption to be ~ 4 W per m^{-2} of the device area.[47] Assuming that a liquid-crystal-based device is kept transparent for half of the day (6 hours), the energy usage is 86.4 KJ m^{-2}.

Assuming that all the designs considered in this section are switched just twice during the day (say from transparent to white and back), then accounting for the 2x switching energy for the other designs, the figure of merit is:

$\eta_{LC} = 2 \times 5.9 \times 10^{-6} J^{-1} m^{-2}$ or $0.007\ \eta_{PPC}$

It follows that for this ideal case scenario, the PPC-based design is several times more effective at modulating solar energy than notable electrochromic and electrodeposition-based designs, and orders of magnitude more effective than liquid-crystal-based designs. However, in real scenarios, the switching energy of PPC-based devices would depend on the pumping system, friction in the plumbing, and the device geometry. It is beyond our expertise to accurately quantify the effects of these factors in detail. Nonetheless, as an approximation, if a pump with 20% efficiency is used to pump liquid or air into the PPC-based system, η_{PPC} would be reduced to a level close to that of $\eta_{Electrodep}$ and $\eta_{Electrochrom}$. It is therefore reasonable to say that in practice, the η of PPC-based designs are comparable to those of notable electrochromic and electrodeposition-based, and significantly higher than those of liquid crystal-based designs.

References

1. Mandal, J., Fu, Y., Overvig, A.C., Jia, M., Sun, K., Shi, N.N., Zhou, H., Xiao, X., Yu, N., and Yang, Y. (2018). Hierarchically porous polymer coatings for highly efficient passive daytime radiative cooling. Science *362*, 315.

2. Choi, S.H., Kim, S.-W., Ku, Z., Visbal-Onufrak, M.A., Kim, S.-R., Choi, K.-H., Ko, H., Choi, W., Urbas, A.M., Goo, T.-W., *et al.* (2018). Anderson light localization in biological nanostructures of native silk. Nature Communications *9*, 452.

3. Mandal, J., Du, S., Dontigny, M., Zaghib, K., Yu, N., and Yang, Y. (2018). Li4Ti5O12: A Visible-to-Infrared Broadband Electrochromic Material for Optical and Thermal Management. Advanced Functional Materials *28*, 1802180.

4. Tong, J.K., Huang, X., Boriskina, S.V., Loomis, J., Xu, Y., and Chen, G. (2015). Infrared-Transparent Visible-Opaque Fabrics for Wearable Personal Thermal Management. ACS Photonics *2*, 769–778.

5. Hsu, P.-C., Song, A.Y., Catrysse, P.B., Liu, C., Peng, Y., Xie, J., Fan, S., and Cui, Y. (2016). Radiative human body cooling by nanoporous polyethylene textile. Science *353*, 1019.

6. Yu, N., Mandal, J., Overvig, A., and Shi, N. (2016). Systems and Methods for Radiative Cooling and Heating. Available at: https://patentscope.wipo.int/search/en/detail.jsf?docId=WO2016205717 [Accessed August 30, 2019].

7. Srinivasan, A., Czapla, B., Mayo, J., and Narayanaswamy, A. (2016). Infrared dielectric function of polydimethylsiloxane and selective emission behavior. Appl. Phys. Lett. *109*, 061905.

8. Granqvist, C.G. (1993). Electrochromic materials: Microstructure, electronic bands, and optical properties. Appl. Phys. A *57*, 3–12.

9. Bessière, A., Marcel, C., Morcrette, M., Tarascon, J.-M., Lucas, V., Viana, B., and Baffier, N. (2002). Flexible electrochromic reflectance device based on tungsten oxide for infrared emissivity control. Journal of Applied Physics *91*, 1589–1594.

10. Li, H., Xie, K., Pan, Y., Yao, M., and Xin, C. (2009). Variable emissivity infrared electrochromic device based on polyaniline conducting polymer. Synthetic Metals *159*, 1386–1388.

11. Li, Z., Zhou, Y., Qi, H., Pan, Q., Zhang, Z., Shi, N.N., Lu, M., Stein, A., Li, C.Y., Ramanathan, S., *et al.* (2016). Correlated Perovskites as a New Platform for Super-Broadband-Tunable Photonics. Advanced Materials *28*, 9117–9125.

12. Chandrasekhar, P., Zay, B.J., Lawrence, D., Caldwell, E., Sheth, R., Stephan, R., and Cornwell, J. (2014). Variable-emittance infrared electrochromic skins combining unique conducting polymers, ionic liquid electrolytes, microporous polymer membranes, and semiconductor/polymer coatings, for spacecraft thermal control. Journal of Applied Polymer Science *131*. Available at: https://onlinelibrary.wiley.com/doi/abs/10.1002/app.40850 [Accessed August 30, 2019].

13. Baetens, R., Jelle, B.P., and Gustavsen, A. (2010). Properties, requirements and possibilities of smart windows for dynamic daylight and solar energy control in buildings: A state-of-the-art review. Solar Energy Materials and Solar Cells *94*, 87–105.

14. Rougier, A., Sauvet, K., and Sauques, L. (2008). Electrochromic materials from the visible to the infrared region: an example WO3. Ionics *14*, 99–105.

15. Monk, P., Mortimer, R., and Rosseinsky, D. (2007). Electrochromism and Electrochromic Devices (Cambridge: Cambridge University Press) Available at: https://www.cambridge.org/core/books/electrochromism-and-electrochromic-devices/535971375B2D61A865DCA15C7A2DA719.

16. Sadman, K., Delgado, D.E., Won, Y., Wang, Q., Gray, K.A., and Shull, K.R. (2019). Versatile and High-Throughput Polyelectrolyte Complex Membranes via Phase Inversion. ACS Appl. Mater. Interfaces *11*, 16018–16026.

17. Syurik, J., Jacucci, G., Onelli, O.D., Hölscher, H., and Vignolini, S. (2018). Bio-inspired Highly Scattering Networks via Polymer Phase Separation. Advanced Functional Materials *28*, 1706901.

18. Ürge-Vorsatz, D., Cabeza, L.F., Serrano, S., Barreneche, C., and Petrichenko, K. (2015). Heating and cooling energy trends and drivers in buildings. Renewable and Sustainable Energy Reviews *41*, 85–98.

19. Wikipedia (2019). Daylighting. Wikipedia. Available at: https://en.wikipedia.org/w/index.php?title=Daylighting&oldid=912974373 [Accessed August 30, 2019].

20. Ander, G. (2016). Daylighting. WBDG - Whole Building Design Guide. Available at: https://www.wbdg.org/resources/daylighting [Accessed July 23, 2019].

21. Farrell, M. (2017). Beat the Summer Heat With Window Coverings. Consumer Reports. Available at: https://www.consumerreports.org/energy-efficiency/beat-the-heat-with-window-coverings/ [Accessed July 23, 2019].

22. Souppouris, A. (2014). Skyscraper concept blocks the sun with hundreds of retractable umbrellas. The Verge. Available at: https://www.theverge.com/2014/4/18/5623776/rex-media-headquarters-concept-photo-essay [Accessed July 23, 2019].

23. Raman, A.P., Anoma, M.A., Zhu, L., Rephaeli, E., and Fan, S. (2014). Passive radiative cooling below ambient air temperature under direct sunlight. Nature *515*, 540–544.

24. Gentle, A.R., and Smith, G.B. (2015). A Subambient Open Roof Surface under the Mid-Summer Sun. Advanced Science *2*, 1500119.

25. Gentle, A.R., and Smith, G.B. (2010). Radiative Heat Pumping from the Earth Using Surface Phonon Resonant Nanoparticles. Nano Lett. *10*, 373–379.

26. Zhai, Y., Ma, Y., David, S.N., Zhao, D., Lou, R., Tan, G., Yang, R., and Yin, X. (2017). Scalable-manufactured randomized glass-polymer hybrid metamaterial for daytime radiative cooling. Science *355*, 1062–1066.

27. Peel, M.C., Finlayson, B.L., and McMahon, T.A. (2007). Updated world map of the Köppen-Geiger climate classification. Hydrology and Earth System Sciences *11*, 1633–1644.

28. Yablonovitch, E., Wudl, F., Dunn, B., Reynolds, J.R., Tanner, D.B., Baughman, R.H., Zakhidov, A.A., and CALIFORNIA UNIV LOS ANGELES (2005). Electrochromic Adaptive Infrared Camouflage. (Ft. Belvoir: Defense Technical Information Center) Available at: http://www.dtic.mil/docs/citations/ADA442555 [Accessed August 30, 2019].

29. Wade, L. Alcohol - Physical properties of alcohols. Encyclopedia Britannica. Available at: https://www.britannica.com/science/alcohol [Accessed July 23, 2019].

30. Schlotter, P., Baur, G.M., Schmidt, R., and Weinberg, U. (1994). Laminated electrochromic device for smart windows. In Optical Materials Technology for Energy Efficiency and Solar Energy Conversion XIII (International Society for Optics and Photonics), pp. 351–362. Available at: https://www.spiedigitallibrary.org/conference-proceedings-of-spie/2255/0000/Laminated-electrochromic-device-for-smart-windows/10.1117/12.185378.short [Accessed August 30, 2019].

31. Kim, D., Lee, E., Lee, H.S., and Yoon, J. (2015). Energy Efficient Glazing for Adaptive Solar Control Fabricated with Photothermotropic Hydrogels Containing Graphene Oxide. Scientific Reports *5*, 7646.

32. Zhou, Y., Cai, Y., Hu, X., and Long, Y. (2014). Temperature-responsive hydrogel with ultra-large solar modulation and high luminous transmission for “smart window” applications. J. Mater. Chem. A *2*, 13550–13555.

33. Kats, M.A., Blanchard, R., Zhang, S., Genevet, P., Ko, C., Ramanathan, S., and Capasso, F. (2013). Vanadium Dioxide as a Natural Disordered Metamaterial: Perfect Thermal Emission and Large Broadband Negative Differential Thermal Emittance. Phys. Rev. X *3*, 041004.

34. Suntuitive (2016). Suntuitive Self Tinting Glass-Technical Information. Suntuitive. Available at: https://suntuitiveglass.com/wp-content/uploads/2018/06/Suntuitive-Technical-Brochure.pdf [Accessed August 30, 2019].

35. Li, X.-H., Liu, C., Feng, S.-P., and Fang, N.X. (2019). Broadband Light Management with Thermochromic Hydrogel Microparticles for Smart Windows. Joule *3*, 290–302.

36. Barile, C.J., Slotcavage, D.J., Hou, J., Strand, M.T., Hernandez, T.S., and McGehee, M.D. (2017). Dynamic Windows with Neutral Color, High Contrast, and Excellent Durability Using Reversible Metal Electrodeposition. Joule *1*, 133–145.

37. Murray, J., Ma, D., and Munday, J.N. (2017). Electrically Controllable Light Trapping for Self-Powered Switchable Solar Windows. ACS Photonics *4*, 1–7.

38. Park, S., and Hong, J.W. (2009). Polymer dispersed liquid crystal film for variable-transparency glazing. Thin Solid Films *517*, 3183–3186.

39. Sani, E., and Dell’Oro, A. (2016). Spectral optical constants of ethanol and isopropanol from ultraviolet to far infrared. Optical Materials *60*, 137–141.

40. Subasi, Y., and Cicek, B. (2017). Recent advances in hydrophilic modification of PVDF ultrafiltration membranes – a review: part II. Membrane Technology *2017*, 5–11.

41. Subasi, Y., and Cicek, B. (2017). Recent advances in hydrophilic modification of PVDF ultrafiltration membranes – a review: part I. Membrane Technology *2017*, 7–12.

42. Zhang, X., Sahraei, E., and Wang, K. (2016). Li-ion Battery Separators, Mechanical Integrity and Failure Mechanisms Leading to Soft and Hard Internal Shorts. Scientific Reports *6*, 32578.

43. Bartok, J. (2015). Plastic Greenhouse Film Update. Center for Agriculture, Food and the Environment. Available at: https://ag.umass.edu/greenhouse-floriculture/fact-sheets/plastic-greenhouse-film-update [Accessed August 30, 2019].

44. Arkema (2017). KYNAR® & KYNAR FLEX® PVDF Performance Characteristics and Data. Arkema.

Available at: https://www.extremematerials-arkema.com/en/product-families/kynar-pvdf-family/download-performance-characteristics-data-brochure [Accessed July 23, 2019].

45. Razak, H.A., Chua, C.S., and Toyoda, H. (2004). Weatherability of coated fabrics as roofing material in tropical environment. Building and Environment *39*, 87–92.

46. Eriksson, T.S., and Granqvist, C.G. (1982). Radiative cooling computed for model atmospheres. Appl. Opt., AO *21*, 4381–4388.

47. Keyoonwong, W., Khan-ngern, W., Ruxsri, P.T.V., and Raksasataya, V. (2018). PDLC film's energy consumption and performance for light filtration system. In 2018 International Conference on Embedded Systems and Intelligent Technology International Conference on Information and Communication Technology for Embedded Systems (ICESIT-ICICTES), pp. 1–4.